Earth Planets Space, **50**, 1047–1054, 1998

Numerical models of convection in a rheologically stratified oceanic upper mantle: Early results

Mamoru Kato

Department of Geophysics, Kyoto University, Kyoto 606-8502, Japan

(Received March 18, 1998; Revised October 30, 1998; Accepted November 4, 1998)

Recent seismological evidences imply that the boundary between the lithosphere and asthenosphere is a compositional boundary in the oceanic upper mantle, and a rapid increase of viscosity at this boundary is suggested. We modeled a thermal convection in the oceanic mantle numerically using the finite element method, and investigated geodynamical consequences of such a rheological layering. Early results from both quasi-steady state flows and time-dependent flows are presented in this report. We assumed a temperature- and depth-dependent viscosity law so that both the thermal effects and those of layering are taken into account. The effect of a high-viscosity layer (HVL) is small on the flow and the temperature field. Velocity gradients in the HVL are small in both directions, and the velocity field is well approximated by a one-dimensional channel flow. The HVL acts as a low-pass filter of the dynamic topography.

1. Introduction

The rheological property of the Earth's mantle can be approximated as viscous when we consider various phenomena in a geological time scale, and a viscous fluid is commonly used in modeling a subsolidus convection in the mantle. Geophysical observations are usually made at the Earth's surface, most of which are sensitive to the shallow structure of the mantle, with a notable exception of the long-wavelength geoid (e.g., Richards and Hager, 1984; Forte *et al.*, 1994), and the behavior of tectonic plates has been extensively studied. In many numerical models, the convection is assumed to be thermally driven, and the plates are modeled as thermal boundary layers (TBLs). When a temperature-dependent viscosity is assumed for the upper mantle, a TBL develops at the surface, which is characterized by a high viscosity, a uniform surface velocity, and a low strain-rate (e.g., King *et al.*, 1992). Observed age-depth relationship of sea-floor is successfully explained by TBL models, except for in the oldest basins (Parsons and Sclater, 1977; Stein and Stein, 1992; McNutt, 1995).

Recently we revealed from seismological observations that the temperature is not the sole control on the thickness of the oceanic lithosphere (Gaherty *et al.*, 1998; Kato and Jordan, 1998). In our regional one-dimensional models, the boundary between the lithosphere and asthenosphere is marked by a negative impedance contrast (G discontinuity), and the G discontinuity is much deeper for the Philippine-Japan corridor in the young Philippine Sea Basin (Kato and Jordan, 1998) than for the Tonga-Hawaii corridor in the old southern Pacific Basin (Gaherty *et al.*, 1996). We then suggested that the G discontinuity is probably a compositional boundary, and its depth is set at the ridge environment (Hirth and Kohlstedt, 1996; Gaherty *et al.*, 1998; Kato and Jordan, 1998). Such a compositional difference between the lithosphere and asthenosphere has been implied in petrology (Ringwood, 1975), but this has not been previously documented seismologically due to low resolution of seismological models in the oceanic region.

The G discontinuity also marks the discontinuous change of water content in the oceanic upper mantle. Due to their high partition coefficients into the basaltic melt, volatiles (e.g., H_2O, CO_2) are efficiently stripped out from the partial melted source mantle, and the residue composes a dry harzburgite layer, which overlays the hydrous but undersaturated peridotite layer. Rheologically, this dry-to-wet transition induces a sharp drop in the viscosity (Karato, 1986; Hirth and Kohlstedt, 1996). The presence of water reduces the viscosity through the enhanced defect mobility in olivine crystals (Karato, 1986), and the viscosity contrast between the lithosphere and asthenosphere is estimated to be more than two orders of magnitude (Hirth and Kohlstedt, 1996). The purpose of this study is to investigate the effects of this viscosity jump in the large scale convection of the oceanic upper mantle. While the effects of the compositional layering beneath cratons have been studied (Kincaid, 1990; Shapiro *et al.*, 1991), this has not been seriously considered for the oceanic mantle. In this study, we are interested in the behavior of the surface boundary layer that is a superposition of thermal and rheological boundary layers. Our approach here is to model and compare a number of simple cases, and we present results of quasi-steady state flow models and subduction models.

2. Numerical

The finite-element code used in this study is based on Conman (King *et al.*, 1990), and is slightly modified for a parallel CPU machine. We divide a 3-by-1 rectangular domain into 3072 (64-by-48) rectangular elements (Fig. 1).

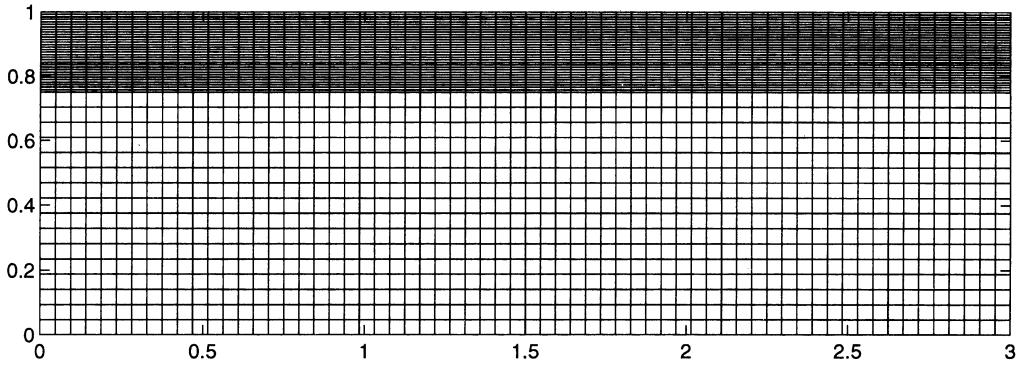

Fig. 1. The finite element grid used in the calculation. A 3-by-1 rectangular box is divided into 3072 (64-by-48) rectangular elements. Node spacing in x-direction is uniform. In z-direction in the upper quarter the node spacing is set to be one sixth of that in the rest of the domain.

The free-slip boundary condition is used for both top and bottom boundaries, and the reflective and free slip (insulating) boundary condition for the side boundaries. A Newtonian rheology law is employed in this study, and the viscosity is assumed to be temperature- and depth-dependent. We used the temperature-dependent law of Gurnis and Hager (1988),

$$\eta = \eta^* \exp[6.215(T_{\rm bot} - T)] \qquad (1)$$

where $T_{\rm bot}$ is the bottom temperature. This gives a 500-fold increase of viscosity over the unit temperature increase (Gurnis and Hager, 1988), and provides a good approximation to the rheological property of olivine (King, 1990). The depth-dependence is used to introduce a high-viscosity layer (HVL); the background viscosity, η^*, in the uppermost mantle is set to be higher than in the rest of the mantle. Transition from the upper mantle to the HVL is then expressed as a discontinuous increase of background viscosity η^* at depth $z_{\rm o}$,

$$\eta^*(z) = \eta_1^* H[z_{\rm o} - z] + \eta_2^* H[z - z_{\rm o}] \qquad (2)$$

where $H[\ ]$ is the Heviside function, and η_1^*, and η_2^* are the background viscosity in the upper mantle and the HVL, respectively. Throughout this report, the Rayleigh number is defined based on η_1^*. Low-viscosity weak zones (width: 0.9375, height: 0.125) are placed at top corners to promote a smooth upwelling and downwelling (Gurnis and Hager, 1988; King *et al.*, 1992). The viscosity of weak zones is fixed to η_1^* so that the viscosity contrast between the plate and weak zone is of order of 10^2.

The domain is both internally and basally heated, and top and bottom temperatures are fixed to 0 and the unit dimensionless temperature, respectively. At $t = 0$, a thin ($\sim$0.05) boundary layer is placed at the surface, and the temperature in the rest of the domain is set to be the unit temperature. A sine-shaped small perturbation (1.0%) is assigned on the initial temperature field over the entire domain to invoke an upwelling at the left side and a downwelling at the right side. Free parameters include the thickness of the HVL ($1 - z_{\rm o}$), the magnitude of viscosity contrast at the boundary (η_2^*/η_1^*), the thermal Rayleigh number (Ra), and the amount of internal heating. Figures are plotted using non-dimensionalized numbers unless otherwise noted. Scaling variables are given in Table 1, which gives the average plate velocity of approximately 4 cm/yr.

Table 1. Scaling variables.

Parameter	Value
Depth of the domain, D	1.0×10^6 m
Temperature contrast, ΔT	1000 K
Reference density, ρ	3.3×10^3 kg m^{-3}
Thermal diffusivity, κ	5.0×10^6 m^{2}s^{-1}
Thermal expansion, α	2.0×10^{-5} K^{-1}
Thermal conductivity	3.0 W m^{-1} K^{-1}
Gravity acceleration, g	10 m s^{-2}
Reference viscosity	$\sim 5 \times 10^{20}$ Pa·s

3. Results

3.1 Quasi steady state flow

Figure 2a shows a temperature field of the quasi steady state flow for the control case (Table 2), in which the HVL is absent ($\eta_2^*/\eta_1^* = 1$). The flow is in the clockwise direction and is smooth, and a thick thermal boundary layer develops at the surface. The temperature field becomes anti-symmetric due to the internal heating, and a weak local convection cell is formed next to the downwelling. Effects of the HVL are small on the global features of the flow field; either when $\eta_2^*/\eta_1^* = 5$ (Fig. 2b) or $\eta_2^*/\eta_1^* = 10$ (Fig. 2c), the temperature field becomes similar to the one for the control case. The entire domain is substantially cooled down, and a well-developed TBL caps the domain. The viscosity contrast between the boundary layer and the rest of the upper mantle is already high due to the thermal effect, and the effect of additional viscosity increase in the HVL appears to be negligible on the flow field. Similar features are also seen when the thickness of the HVL is changed (Figs. 2d–2e), though the temperature in the mantle is slightly higher for the thick HVL case (Fig. 2e) than for the other cases.

Temperature profiles at the center of the domain are almost identical in all cases, but there are differences of the flow velocities and stresses in the uppermost mantle (Fig. 3). Horizontal velocity takes the maximum value at the surface

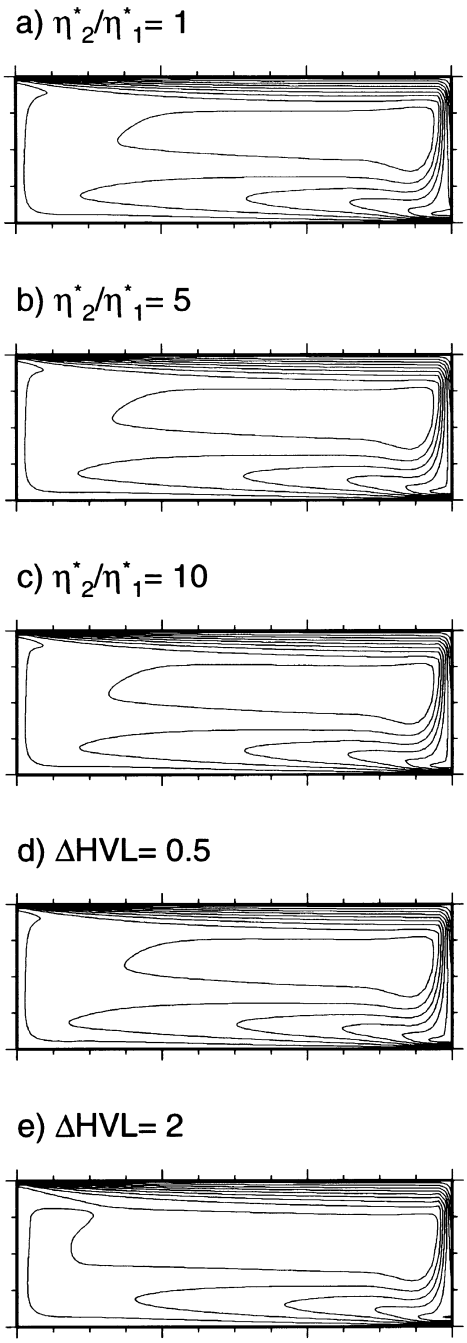

Fig. 2. Contoured image of the temperature fields. Increments of the contour is 0.1 unit temperature. a) The control case Qa1, for which a discontinuous jump of viscosity in the uppermost mantle is not implemented. b), c) Cases Qb1 and Qb5, for which a discontinuous jump, $\eta_2^*/\eta_1^* = 5$ and $\eta_2^*/\eta_1^* = 10$ is implemented approximately at $z = 0.906$, respectively. d), e) Cases Qe1 and Qd1, for which a discontinuous jump $\eta_2^*/\eta_1^* = 5$ is implemented approximately at $z = 0.95$ and 0.81, respectively.

Table 2. Quasi steady state flow models.

Case	Ra	VR	TH	IHF	TS
Qa1	1e6	1	-	55	30,000
Qa2	1e6	1	-	53	60,000
Qa3	1e6	1	-	69	30,000
Qa4	1e6	1	-	71	60,000
Qa5	3e6	1	-	N/A	30,000
Qa6	5e6	1	-	N/A	30,000
Qb1	1e6	5	1.0	55	30,000
Qb2	1e6	5	1.0	53	60,000
Qb3	1e6	5	1.0	68	30,000
Qb4	1e6	5	1.0	70	60,000
Qb5	1e6	10	1.0	55	30,000
Qb6	1e6	10	1.0	53	60,000
Qb7	1e6	10	1.0	70	60,000
Qb8	5e6	5	1.0	62	30,000
Qb9	3e6	5	1.0	59	30,000
Qb10	3e6	5	1.0	N/A	30,000
Qc1	1e6	5	0.25	54	30,000
Qc2	1e6	5	0.25	68	30,000
Qc3	3e6	5	0.25	N/A	30,000
Qd1	1e6	5	2.0	57	30,000
Qd2	1e6	5	2.0	70	30,000
Qd3	3e6	5	2.0	57	30,000
Qd4	1e6	10	2.0	57	30,000
Qe1	1e6	5	0.5	54	30,000
Qe2	1e6	5	0.5	68	30,000
Qe3	5e6	5	0.5	59	30,000
Qe5	3e6	5	0.5	56	30,000
Qf1	1e6	5	0.75	54	30,000
Qf2	1e6	5	0.75	68	30,000
Qf3	5e6	5	0.75	57	30,000
Qf4	3e6	5	0.75	61	30,000

Ra: Thermal Rayleigh number. VR: η_2^*/η_1^*. TH: Thickness of the HVL. Thickness is normalized by the unit thickness, which is arbitrarily chosen as 0.09375. IHF: Internal heating fraction. N/A indicates that the flow is turbulent and did not reach a steady state. TS: Total time steps.

($z = 1.0$) and then decreases as the depth increases. For the control case, velocity gradient, $\partial V_x/\partial z$, is also a smooth function of depth (Fig. 3); $\partial V_x/\partial z$ increases gradually as the depth increases and there is no first order discontinuity in the velocity profile. In contrast, for cases with the HVL, $\partial V_x/\partial z$ is very small and almost constant in the HVL, but at the lower boundary of the HVL, $\partial V_x/\partial z$ increases discontinuously. Gradients of the plate velocity at the surface, $\partial V_x/\partial x$, are also small. Smaller $|\partial V_x/\partial z|$ and $|\partial V_x/\partial x|$ in the boundary layer are common features of the HVL cases.

When the HVL is imposed, τ_{xx}^D increases discontinuously at the rheological boundary, which reflects an increase of viscosity at this depth. On the other hand, change of τ_{xz} is smooth across this boundary. In the boundary layer, the flow is dominantly horizontal and it is primarily in horizontal

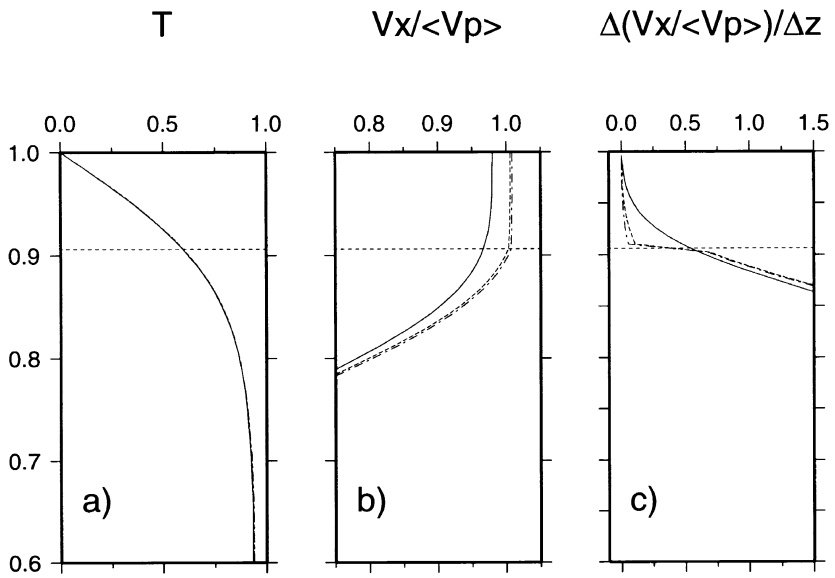

Fig. 3. Profiles of temperature (a), flow velocity (b), and their gradients (c) for cases Qa1 (control case; solid line), Qb1 (η_2^*/η_1^*=5; dashed line), and Qb5 (η_2^*/η_1^*=10; dash-dot line). Flow velocity is normalized by the average plate velocity, which is defined as an average of at surface nodes (at $z = 1.0$) except two corner nodes. Temperature fields are identical for three cases. The horizontal dash line indicates the depth of rheological boundary for cases Qb1 and Qb5.

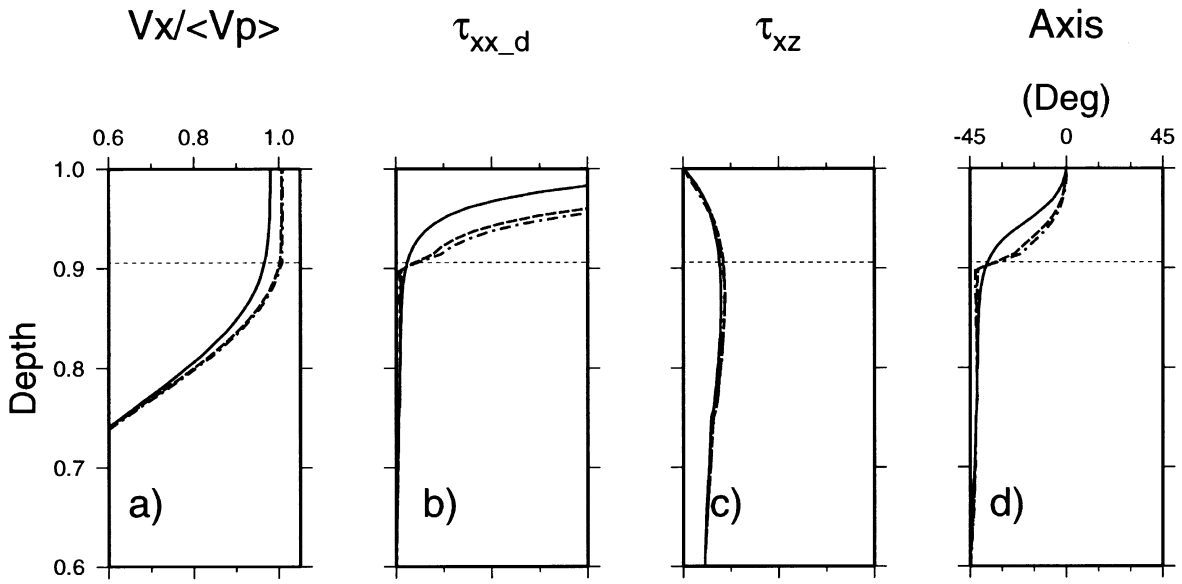

Fig. 4. Profiles of normalized flow velocity (a), and two stress components, τ_{xx}^D (b), and τ_{xz} (c), and direction of the maximum compression axis (d) for cases Qa1 (solid line), Qb1 (dashed line), and Qb5 (dash-dot line). The horizontal dash line indicates the depth of rheological boundary for cases Qb1 and Qb5. Stresses are plotted in the same scale.

tension for all cases. For the control case, τ_{xx}^D is smoothly decreasing and τ_{xz} smoothly increasing, and the direction of the maximum compression stress axis then shifts gradually from vertical to an oblique angle (Fig. 4). For the HVL cases, the direction of the maximum compression rapidly and discontinuously changes at the HVL boundary due to the discontinuous large change of τ_{xx}^D. This rapid change of direction indicates a discontinuous change of the stress field between the lithosphere and asthenosphere.

Such observations of velocity gradients and stresses could be understood with one-dimensional channel flow models (e.g., Turcotte and Schubert, 1982, pp. 232–236). In a simple case of two-layer Couette flow with constant viscosities, for example, velocities and shear stress are continuous at the boundary of two layers. The velocity gradient in each layer is inversely proportional to the viscosity, and thus it become small in the high-viscosity layer. In our models, viscosities varies over depths in layers, but the viscosity contrast be-

Table 3. Time-dependent flow models.

Case	Ra	VR	TH	IH	TS
Sa1	1e6	1	-	-	5,000
Sa2	1e6	1	-	Low	5,000
Sa3	1e6	1	-	High	5,000
Sa4	3e6	1	-	-	5,000
Sa5	3e6	1	-	Low	5,000
Sa6	3e6	1	-	High	5,000
Sa7	5e6	1	-	-	5,000
Sa8	5e6	1	-	Low	5,000
Sa9	5e6	1	-	High	5,000
Sb1	1e6	5	0.25	-	5,000
Sb2	1e6	5	0.25	Low	5,000
Sb3	1e6	5	0.25	High	5,000
Sb4	3e6	5	0.25	-	5,000
Sb5	3e6	5	0.25	Low	5,000
Sb6	3e6	5	0.25	High	5,000
Sb7	5e6	5	0.25	-	5,000
Sb8	5e6	5	0.25	Low	5,000
Sb9	5e6	5	0.25	High	5,000
Sc1	1e6	5	0.5	-	5,000
Sc2	1e6	5	0.5	Low	5,000
Sc3	1e6	5	0.5	High	5,000
Sc4	3e6	5	0.5	-	5,000
Sc5	3e6	5	0.5	Low	5,000
Sc6	3e6	5	0.5	High	5,000
Sc7	5e6	5	0.5	-	5,000
Sc8	5e6	5	0.5	Low	5,000
Sc9	5e6	5	0.5	High	5,000
Sd1	1e6	5	1.0	-	5,000
Sd2	1e6	5	1.0	Low	5,000
Sd3	1e6	5	1.0	High	5,000
Sd4	3e6	5	1.0	-	5,000
Sd5	3e6	5	1.0	Low	5,000
Sd6	3e6	5	1.0	High	5,000
Sd7	5e6	5	1.0	-	5,000
Sd8	5e6	5	1.0	Low	5,000
Sd9	5e6	5	1.0	High	5,000

Table 3. (continued).

Case	Ra	VR	TH	IH	TS
Se1	1e6	5	2.0	-	5,000
Se2	1e6	5	2.0	Low	5,000
Se3	1e6	5	2.0	High	5,000
Se4	3e6	5	2.0	-	5,000
Se5	3e6	5	2.0	Low	5,000
Se6	3e6	5	2.0	High	5,000
Se7	5e6	5	2.0	-	5,000
Se8	5e6	5	2.0	Low	5,000
Se9	5e6	5	2.0	High	5,000

Ra: Thermal Rayleigh Number. VR: η_2^*/η_1^*. TH: Thickness of the HVL. Thickness is normalized by the unit thickness, which is arbitrarily chosen as 0.09375. IH: Amount of internal heating. As the flow is not steady state it is not possible to quantify the internal heating fraction.

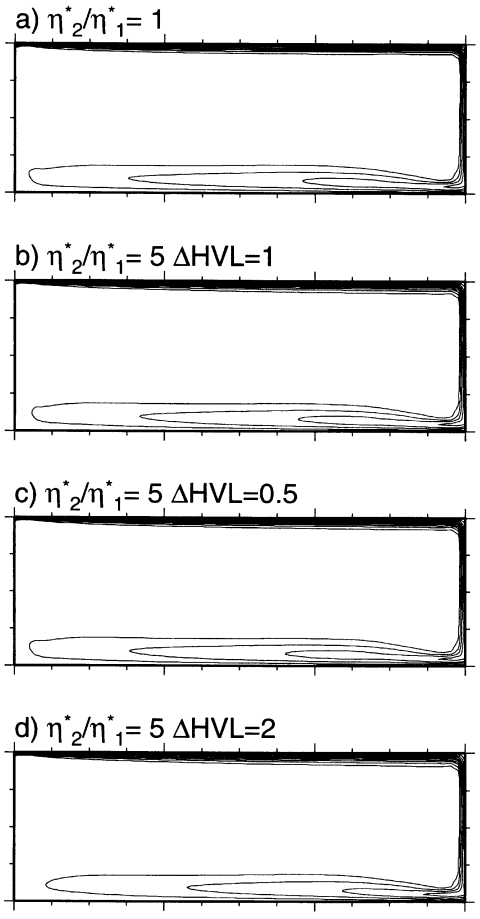

Fig. 5. Contoured image of the temperature fields. Increments of the contour is 0.1 unit temperature. a) Case Sa1 (the control case), b) Sd1 ($\eta_2^*/\eta_1^* = 5$), c) Sc1 (a thin HVL), and d) Se1 (a thick HVL).

tween the rigid plate and soft upper mantle is large so that the velocity gradients become small in the HVL. In previous convection models with a temperature-dependent rheology, the transition between the plate and the upper mantle is gradual, and there in no clear boundary. By introducing the HVL, we have a clear definition of plate based on velocities and stresses even in a simple Newtonian rheology model.

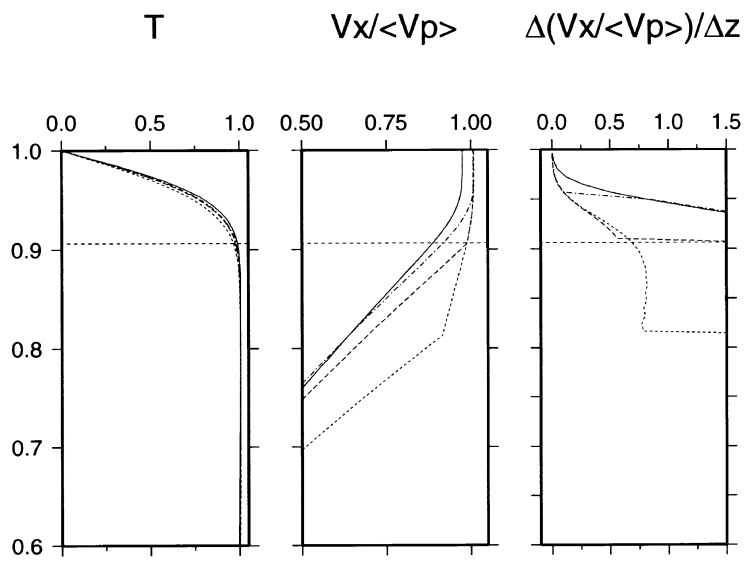

Fig. 6. Profiles of temperature, normalized flow velocity, and viscosity, and velocity gradient for cases with $Ra = 3 \times 10^6$. Shown are cases Sa4 (the control case; solid line), Sd4 ($\eta_2^*/\eta_1^* = 5$; long dashed line), Sc4 (a thin HVL case; dash-dot line), and Se4 (a thick HVL case; short dashed line).

3.2 Time-dependent flow

In the quasi-steady state flow models, the entire domain is cooled down substantially, and the TBL becomes very thick at the surface. In the convection models of the upper mantle, the base of lithosphere is often defined as the isothermal line of 0.9 dimensionless unit temperature (e.g., Gurnis and Hager, 1988). On the case Qb1 (Fig. 2b), for example, the ratio of thicknesses of the TBL and the HVL exceeds 3. By using a higher Rayleigh number it is possible to make a thinner TBL, but and it is difficult to model a quasi steady state flow since the flow becomes turbulent. Instead, we model the initial stages of the subduction and investigate flow field for thin TBL cases. Two-dimensional time-dependent models have been successfully used and have provided insights on processes in the upper mantle (e.g., Christensen, 1984; Gurnis and Hager, 1988; Chen and Morgan, 1990; Weinstein and Olson, 1992).

A similar model set-up and initial conditions that are used for the quasi steady state cases are used for the time-dependent flow models. An additional low viscosity weak zone of the same size is placed in the lower right corner of the domain (King and Hager, 1990), and the viscosity of these three weak zones is fixed to η_1^*. A thin thermal boundary layer is placed at the top at $t = 0$. Several different combinations of parameters are tested, changing the amount of heat flow and the Rayleigh number (Table 3). The amount of internal heating does not have a large effect on the flow field; the effect of internal heating is mostly to enhance upwelling, but when the flow is still in the early stage the governing process is the cooling at the surface of the domain and the flow field is dominated by the downwelling. The thickness of the TBL is a function of the Rayleigh number but otherwise the thermal fields are similar for all cases modeled here. The flow field is characterized by a skewed velocity distribution, which also shows the dominant effect of slab pull force (Fig. 5). Temperature fields are similar among all cases, and the addition of the HVL has a little effect on the temperature field, which agrees with the results of quasi steady state flows. Vertical and horizontal variations of flow velocity are smaller for rheologically layered cases (Fig. 6), which also agrees with quasi steady state flow cases. In general, characteristics of flows are similar for the quasi steady state flow and time dependent flow cases.

Exceptions are the thin-TBL-thick HVL cases; depth profiles of flow velocity for the thin the TBL case (Sc4) appear to be similar to the non-HVL control case (Sa4) in the uppermost mantle, indicating a lack of control by the rheological layering on the shallow flow field. When the HVL is thicker than the TBL (case 4), it is rheologically uniform at depths of rapid increase of temperature so that the TBL can be viewed as a local phenomenon in a locally homogeneous mantle. A similar feature should occur in a quasi steady state flow with a thin TBL; velocities and stresses are mainly controlled by the temperature.

4. Discussion

Previously, we compared two oceanic models, PA5 for the central Pacific (Gaherty *et al.*, 1996) and PHB3 for the western Philippine Sea (Kato and Jordan, 1998) and discussed the nature of the boundary layer in the oceanic upper mantle. To correct the differences of the sea-floor ages, we applied an empirical scaling relation between shear-wave velocity and temperature (Kato, 1997), assuming that the thermal structure in the uppermost mantle is not affected by the compositional layering. We found that the effect of the rheological layering is small on the thermal structure so that the use of this correction is justified. On one hand, Hirth and Kohlstedt (1996) attributed the flattening of age-sea-floor depth curve to secondary small scale convection below the compositional boundary layer in the older basin (e.g., Richter and Parsons, 1975; Katzman *et al.*, 1998), but this hypothesis is not tested dynamically in this study.

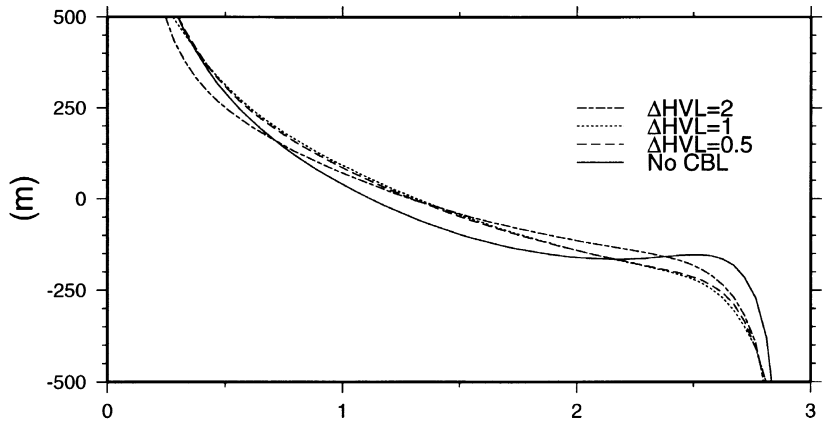

Fig. 7. Dynamic topography calculated from the stress field for cases Qa1 (the control case; solid line), Qb1 (a HVL case; dotted line), Qd1 (a thick HVL case; dash-dotted line), and Qe1 (a thin HVL case; dashed line). Dimensionalized numbers are used in this figure.

One effect of the HVL is the small deformation rate in the lithosphere. Anisotropy in the upper mantle is likely to be due to the lattice preferred orientation (LPO) of olivine, and the lithospheric anisotropy is probably formed by the paleostrain at the ridge environment and fossilized in the lithosphere. Observations of shallow anisotropy in the oceanic upper mantle imply that the oceanic lithosphere maintains the fabric that is formed during the early stage (e.g., Karato, 1989). The small deformation rate in the HVL is favorable to keep such microstructure in the uppermost mantle.

Anisotropy in the LVZ as well as in the lid is required in some recent seismological models (Gaherty *et al.*, 1998; Kato and Jordan, 1998). Origin of such anisotropy in the asthenosphere is ambiguous, but LPO of olivine should represent the past (Ribe, 1989; Zhang and Karato, 1995), or the ongoing accumulation of strain (Montagner and Tanimoto, 1991; Katzman *et al.*, 1998). In a recent model of non-Newtonian viscous flow, the major contribution of anisotropy in the oceanic mantle is estimated from the asthenosphere where the effective viscosity is low (Tommasi *et al.*, 1996). Based on the results of the HVL models in this study, it is suggested that in the rheologically stratified upper mantle, development of a strong shear zone strain could be confined in the asthenosphere, and its width could be narrow. Origin and properties of anisotropy in the asthenosphere then could be different from those in the lithosphere.

Observed sea-floor depth is a superposition of the dynamic topography onto the static age dependent subsidence resulting from growth of the TBL (Kido and Seno, 1994). A large deviation from the predicted age-depth curve often indicates a regional tectonic deformation, such as a massive plume in the south central Pacific (McNutt and Fischer, 1987; McNutt and Judge, 1990). Figure 7 shows calculated dynamic topography at the surface for the quasi steady state cases, following the method of McKenzie *et al.* (1974) (see also Zhong *et al.*, 1993). For the control case, a small local high of dynamic topography appears at approximately $x = 2.7$, which corresponds to a small and weak convection cell beneath it. This local high does not appear for cases with the HVL, for which the dynamic topography is changing smoothly over the domain and is thus relatively rich in the long wavelength component. Dominance of long wavelength components is probably owing to a large viscosity contrast at the rheological boundary which makes the lithosphere difficult to be deformed in a short wavelength. The HVL thus acts as a low-pass filter of the dynamic topography. A large sea-floor depth anomaly in the Philippine Sea is characterized as a uniform subsidence (Park *et al.*, 1990). The Philippine Sea plate is surrounded by active subduction zones, and the downward forces that are exerted at the boundaries of the Philippine Sea plate could account for the subsidence of the basins in the Philippine Sea. Of the dynamic topography due to the subductions, short wavenumber components should be filtered out, but the resultant dominant long wavelength component might contribute to a uniform subsidence of the small Philippine Sea plate. The oceanic lid in the western Philippine Sea is thick (Kato and Jordan, 1998), but it would be difficult to estimate the thickness of the HVL from observed topography as the effect of HVL thickness on the variation of the dynamic topography is small.

5. Concluding Remarks

We modeled mantle convection with the presence of a HVL in the oceanic upper mantle, and investigated the effect of a rheological layering on the mantle convection. A Newtonian rheology law is assumed and a temperature-dependent viscosity is employed so that the effects of both the thermal effects and those of rheological layering on the surface boundary layer are considered. Effect of the rheological layering is negligible on the temperature field, and geophysical observations that are sensitive to the thermal structure cannot distinguish homogeneous and HVL models. Flow velocities are uniform in the HVL, suggesting a small deformation rate in the lithosphere. A sharp transition could exist in the stress field for the matured oceanic upper mantle. Formation of anisotropy in the asthenosphere could have a little effect on the existing lithospheric anisotropy.

Rheological layering is only one aspect of the oceanic compositional boundary layer, and there are several points that should be pursued in future studies. For example, the

evolution of the compositional boundary layer is not considered in this study. Melting differentiation processes at ridges supply the material to this layer, and the chemical and dynamic processes should be important in the organization of the flow and the surface boundary layer in the young oceanic basins. It also should be pointed out that we did not consider the non-Newtonian rheology and the viscous heating (Karato and Wu, 1993; Karato, 1995). It is desirable to utilize a more realistic rheology law and to include small scale processes, especially chemical processes in modeling convective flows in the oceanic upper mantle.

Acknowledgments. The author would like to acknowledge Brad Hager, Steve Shapiro, Mark Simons, and Jim Gaherty for helping him to learn Conman, Shun Karato, Rafi Katzman for their comments on the oceanic compositional boundary layer. He also thanks two anonymous reviewers and the editor, Alessandro M. Forte, for constructive comments to the original manuscript. GMT (Wessel and Smith, 1991) is extensively used in the study. Part of computation was performed at the Earthquake Information Center of Earthquake Research Institute, the University of Tokyo. MK is financially supported by JSPS through the fellowship program.

References

Chen, Y. and J. W. Morgan, A non-linear rheology model for mid-ocean ridge axis topography, *J. Geophys. Res.*, **95**, 17583–17604, 1990.

Christensen, U. R., Convection with pressure- and temperature-dependent non-Newtonian rheology, *Geophys. J. R. Astr. Soc.*, **77**, 343–384, 1984.

Forte, A. M., R. L. Woodward, and A. M. Dziewonski, Joint inversion of seismic and geodynamical data for models of three-dimensional mantle heterogeneity, *J. Geophys. Res.*, **99**, 21857–21977, 1994.

Gaherty, J. B., T. H. Jordan, and L. S. Gee, Depth extent of polarization anisotropy in western Pacific upper mantle, *J. Geophys. Res.*, **101**, 22291–22309, 1996.

Gaherty, J. B., M. Kato, and T. H. Jordan, Seismological structure of the upper mantle: a regional comparison of seismic layering, *Phys. Earth Planet. Sci.*, 1998 (in press).

Gurnis, M. and B. H. Hager, Controls on the structure of subducting slabs, *Nature*, **355**, 317–321, 1988.

Hirth, G. and D. L. Kohlstedt, Water in the oceanic upper mantle: Implication for rheology, melt extraction, and the evolution of the lithosphere, *Earth Planet. Sci. Lett.*, **144**, 93–108, 1996.

Karato, S.-I., Does partial melting reduce the creep strength of the upper mantle?, *Nature*, **319**, 309–310, 1986.

Karato, S.-I., Seismic anisotropy: mechanisms and tectonic implication, in *Rheology of the Solid and of the Earth*, edited by S.-I. Karato and M. Toriumi, pp. 393–422, Oxford University Press, Oxford, 1989.

Karato, S.-I., Effect of water on seismic wave velocities in the upper mantle, *Proc. Japan Academy*, **71**, Ser. B, 61–66, 1995.

Karato, S.-I. and P. Wu, Rheology of the upper mantle: a synthesis, *Science*, **260**, 771–778, 1993.

Kato, M., An analysis of temperature derivative of shear-wave velocity in oceanic lithosphere in the Pacific basin, *J. Phys. Earth*, **45**, 67–71, 1997.

Kato, M. and T. H. Jordan, Seismic structure of the upper mantle beneath the western Philippine Sea, *Phys. Earth Planet. Int.*, 1998 (in press).

Katzman, R., L. Zhao, and T. H. Jordan, High-resolution, two-dimensional vertical tomography of the central Pacific mantle using *ScS* reverberations and frequency-dependent travel times, *J. Geophys. Res.*, **103**, 17933–17971, 1998.

Kido, M. and T. Seno, Dynamic topography compared with residual depth anomalies in oceans and implication for age-depth curve, *Geophys. Res. Lett.*, **21**, 717–720, 1994.

Kincaid, C., The dynamic interaction between tectosphere and large scale mantle's convection, *EOS Trans. AGU*, **71**, 1626, 1990.

King, S. D., The interaction of subducting slab and the 670 km discontinuity, Ph.D. Thesis, Calif. Inst. Tech., Pasadena, 1990.

King, S. D. and B. H. Hager, The relationship between plate velocity and trench viscosity in Newtonian and power-law subduction calculations, *Geophys. Res. Lett.*, **17**, 2409–2412, 1990.

King, S. D., A. Raefsky, and B. H. Hager, Conman: Vectorizing a finite element code for incompressive two-dimensional convection in the earth's mantle, *Phys. Earth Planet. Sci.*, **59**, 196–208, 1990.

King, S. D., C. W. Gable, and S. A. Weinstein, Models of convection-driven tectonic plates: a comparison of models and results, *Geophys. J. Int.*, **109**, 481–487, 1992.

McKenzie, D. P., J. M. Roberts, and N. O. Weiss, Convection in the earth's mantle: towards a numerical simulation, *J. Fluid. Mech.*, **62**, 465–538, 1974.

McNutt, M. K., Marine geodynamics: Depth-age revisited, *Rev. Geophys.*, Suppl., 413–418, 1995.

McNutt, M. K. and K. M. Fischer, The South Pacific superswell, in *Seamounts, Islands, and Atolls*, edited by B. H. Keating, P. Fryer, R. Batiza, and G. W. Boehlert, pp. 25–34, Am. Geophys. Un., Washington, 1987.

McNutt, M. K. and A. V. Judge, The superswell and mantle dynamics beneath the south Pacific, *Science*, **248**, 969–975, 1990.

Montagner, J.-P. and T. Tanimoto, Global upper mantle tomography of seismic velocity and anisotropy, *J. Geophys. Res.*, **96**, 20337–20351, 1991.

Park, C.-H., K. Tamaki, and K. Kobayashi, Age-depth correlation of the Philippine Sea back-arc basins and other marginal basins in the world, *Tectonophys.*, **181**, 351–371, 1990.

Parsons, B. and J. G. Sclater, An analysis of the variation of the ocean floor bathymetry and heat flow with age, *J. Geophys. Res.*, **82**, 803–827, 1977.

Ribe, N. M., On the relation between seismic anisotropy and mantle flow, *J. Geophys. Res.*, **94**, 4213–4223, 1989.

Richards, M. A. and B. H. Hager, Geoid anomalies in a dynamic Earth, *J. Geophys. Res.*, **89**, 5987–6002, 1984.

Richter, F. M. and B. Parsons, On the interaction of two scales of convection in the mantle, *J. Geophys. Res.*, **80**, 2529–2541, 1975.

Ringwood, A. E., *Composition and petrology of the Earth's mantle*, 604 pp., McGraw-Hill, New York, 1975.

Shapiro, S. S., B. H. Hager, and T. H. Jordan, Stability of the continental tectosphere, *EOS Trans. AGU*, **72**, 267, 1991.

Stein, C. and S. Stein, A model for the global variation in oceanic depth and heat flow with lithospheric age, *Nature*, **359**, 123–129, 1992.

Tommasi, A., A. Vauchez, and R. Russo, Seismic anisotropy in ocean basins: Resistive drag of sublithospheric mantle?, *Geophys. Res. Lett.*, **23**, 2991–2994, 1996.

Turcotte, D. L. and G. Schubert, *Geodynamics: Applications of Continuum Physics to Geological Problems*, 450 pp., John Wiley and Sons, New York, 1982.

Weinstein, S. A. and P. L. Olson, Thermal convection with non-Newtonian plates, *Geophys. J. Int.*, **111**, 515–530, 1992.

Wessel, P. and W. H. F. Smith, Free software helps map and display data, *EOS Trans. AGU*, **72**, 441, 445–446, 1991.

Zhang, S. and S.-I. Karato, Lattice preferred orientation of olivine in simple shear deformation and the flow geometry of the upper mantle of the Earth, *Nature*, **375**, 774–777, 1995.

Zhong, S., M. Gurnis, and G. Hulbert, Accurate determination of surface normal stress in viscous flow from a consistent boundary flux model, *Phys. Earth Planet. Sci.*, **78**, 1–8, 1993.

M. Kato (e-mail: mkato@kugi.kyoto-u.ac.jp)